Supplementary Information

Nanoporous Immunoprotective Device for Stem Cell Derived β Cell Replacement Therapy

Ryan Chang[1], Gaetano Faleo[3], Holger A. Russ[4,5], Audrey V. Parent[4], Susanna K. Elledge[2], Daniel A. Bernards[2], Jessica L. Allen[2], Karina Villanueva[4], Matthias Hebrok[4], Qizhi Tang[3,4], Tejal A. Desai[1,2]

[1]UCSF-UC Berkeley Joint PhD Program in Bioengineering, San Francisco, CA, USA

[2]Department of Bioengineering and Therapeutic Sciences, University of California, San Francisco, San Francisco, CA, USA

[3]Department of Surgery, University of California, San Francisco, San Francisco, CA, USA

[4]Diabetes Center, University of California San Francisco, San Francisco, CA, USA

[5]Current address: Barbara Davis Center for Diabetes, University of Colorado, School of Medicine, Aurora, CO, USA.

SUPPLEMENTATRY FIGURES

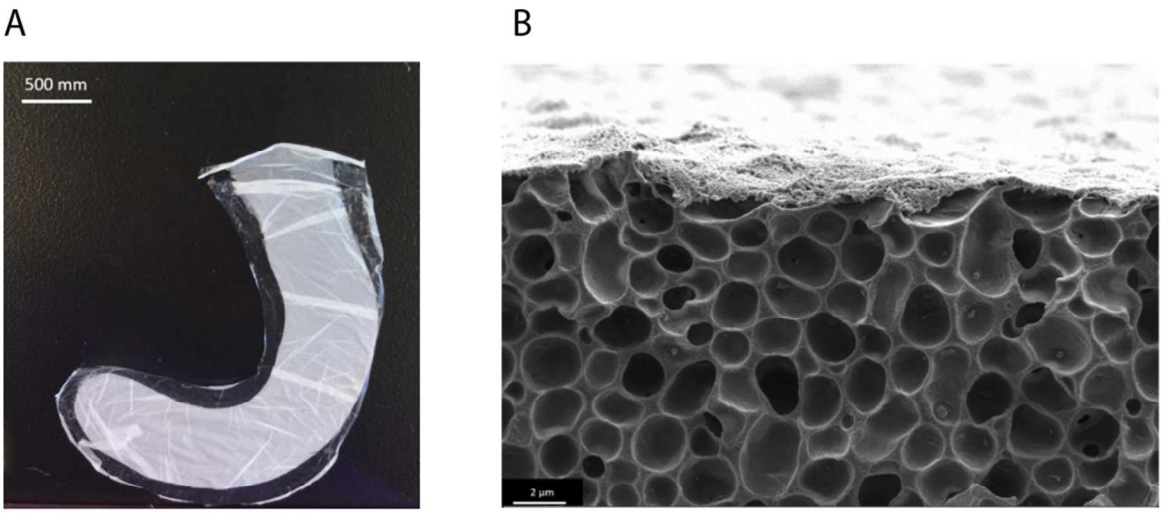

Fig. S1, Fabrication of nanoporous cell encapsulation device. **a**, Gross image of assembled kidney shaped bilaminar cell encapsulation device with well localized clear margins are heat sealed. **b**, Scanning Electron Micrograph of cross section of nanoporous membranes.

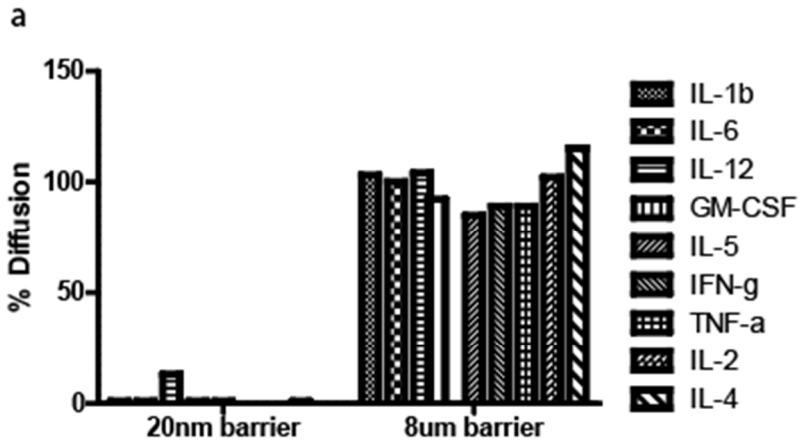

Fig. S2, **Cytokine diffusion across immunoprotective barrier after splenocyte-islet transwell culture. a,** Luminex quantification of mouse-proinflammatory cytokine diffusion rate across 20 nm pore size PCL films and 8 μm pore size PTFE films from the basolateral activated splenocyte containing compartment into the apical islet compartment.

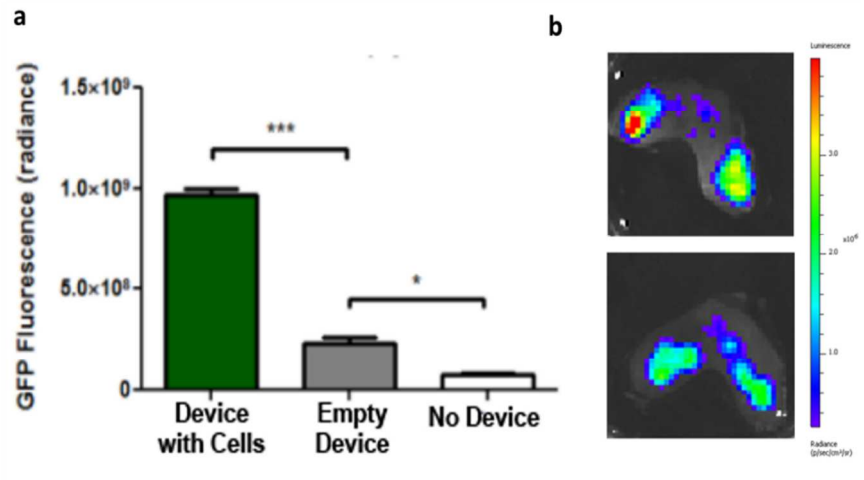

Fig. S3, Evaluation of GFP fluorescence intensity of encapsulated human stem cell derived beta cell clusters (hES-βC) containing GFP reporter driven under the endogenous insulin

promoter. **a,** GFP fluorescence was measured by *in vivo* imaging system (Caliper) from device encapsulated with hES-βC, devices without any cells, and no device background control. (n=4) **b**, live cell luciferase bioluminescence imaging through device demonstrating encapsulated cells are viable and well distributed throughout the cavity of the bilaminar device.

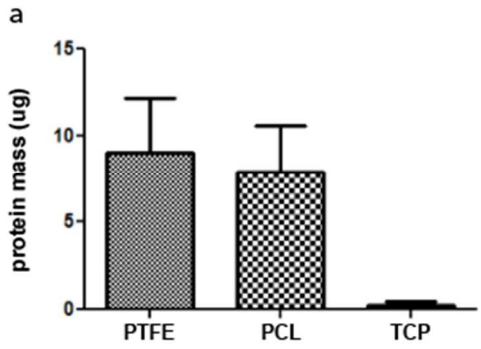

Fig. S4, **Characterization of protein adsorption on material surfaces**. **a,** Quantification of protein mass adsorbed onto 1.5 cm diameter PTFE, PCL, or tissue culture plastic (TCP) material surfaces following 24 hours of incubation in fetal bovine serum. (n=14)

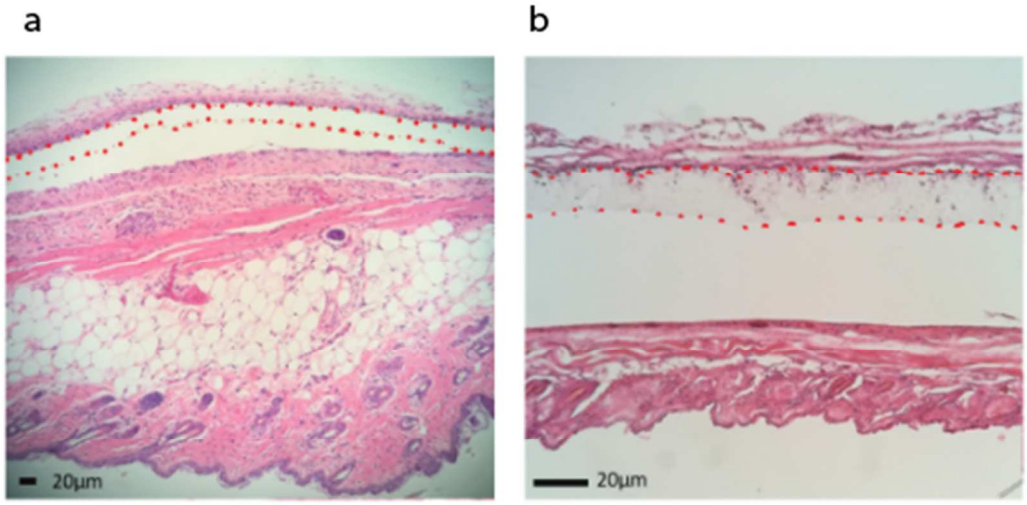

Fig. S5, Assessment of biocompatibility following subcutaneous implantation. **a,** H&E staining of polypropelene films implanted subcutaneously into immunocompetent C57BL/6J mice for 2 weeks. **b,** H&E staining of polycaprolactone thin films implanted subcutaneously into immunocompetent C57BL/6J mice for 4 months.

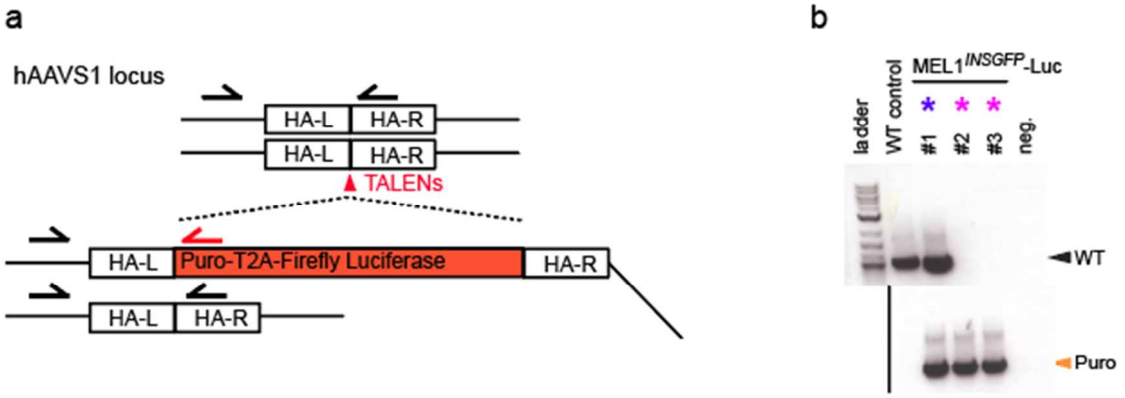

Fig. S6, Generation of hES$^{INS\text{-}GFP;AAVS1\text{-}LUC}$ cell line. a. Schematic illustrating the targeting strategy employed. b. gDNA PCR analysis with primers specific for the wild type (WT, black arrows) AAVS1 DNA sequence and site specific integrated Puro-T2A-Luc donor plasmid (Puro, black and red arrows). WT control is gDNA from hES$^{INS\text{-}GFP}$ cells, no template control is neg. Blue and pink stars indicate heterogeneous (#1) and homologous clones (#2, and #3), respectively.

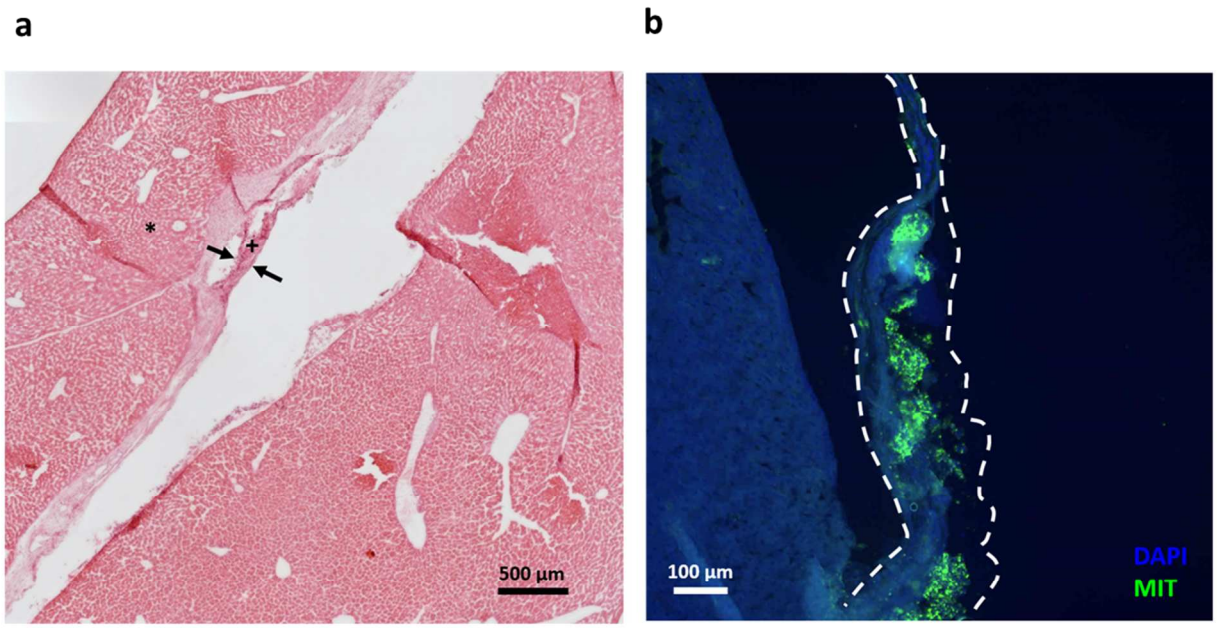

Fig. S7, Histological analysis of teratoma cells confined by device. a, H&E staining of explanted tissue section showing confinement of human teratoma cells within confines of device. Asterisk marks mouse liver tissue, plus marks the human teratoma cells and the solid arrows point to the margins of the device. **b**, immunostaining of explanted tissue sections with human specific anti-mitochondrial antibody. White dotted lines mark the margins of the device.

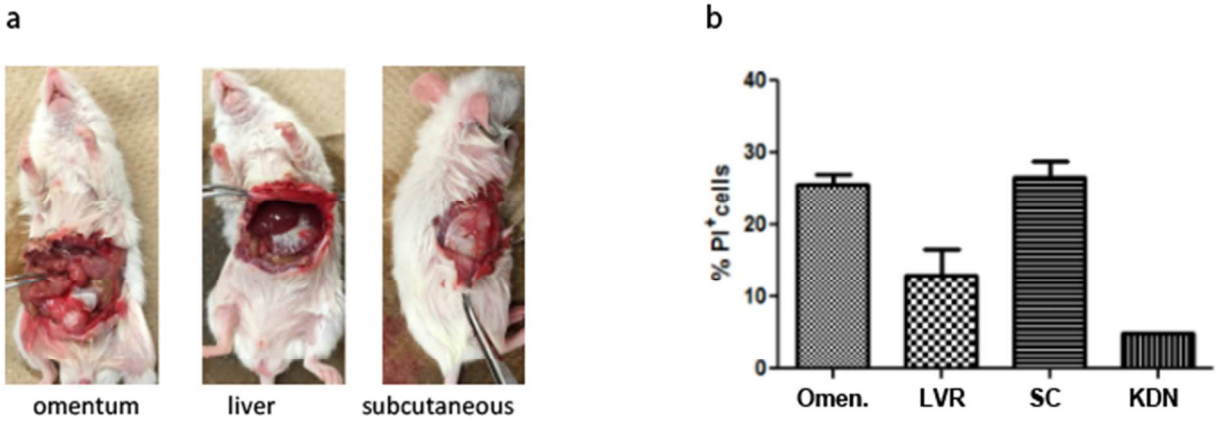

Fig. S8, Assessment of optimal transplant site for NID encapsulated hES-βC. **a,** representative image of NID transplanted in the omentum(Omen.), liver(LVR), subcutaneous

space (SC). **b,** propidium iodine staining of retrieved cells from NID following 1 week transplantation. (n=3)